THE TRIPLE POINT PARADOX FOR THE NONLINEAR WAVE SYSTEM[*]

ALLEN M. TESDALL[†], RICHARD SANDERS[‡], AND BARBARA L. KEYFITZ[†]

Abstract. We present numerical solutions of a two-dimensional Riemann problem for the *nonlinear wave system* which is used to describe the Mach reflection of weak shock waves. Robust low order as well as high resolution finite volume schemes are employed to solve this equation formulated in self-similar variables. These, together with extreme local grid refinement, are used to resolve the solution in the neighborhood of an apparent but mathematically inadmissible shock triple point. Rather than observing three shocks meeting in a single standard triple point, we are able to detect a primary triple point containing an additional wave, a centered expansion fan, together with a sequence of secondary triple points and tiny supersonic patches embedded within the subsonic region directly behind the Mach stem. An expansion fan originates at each triple point. It is our opinion that the structure observed here resolves the von Neumann triple point paradox for the nonlinear wave system. These solutions closely resemble the solutions obtained in [A. M. Tesdall and J. K. Hunter, *SIAM J. Appl. Math.*, 63 (2002), pp. 42–61] for the unsteady transonic small disturbance equation.

Key words. weak shock reflection, self-similar solutions, nonlinear wave system, two-dimensional Riemann problems, von Neumann paradox

AMS subject classifications. 65M06, 35L65, 76L05

DOI. 10.1137/060660758

1. Introduction. Experiments in which a weak shock wave reflects off a thin wedge appear to show a pattern of reflection in which three shocks meet at a triple point. However, the von Neumann theory of shock reflection [11] shows that Mach reflection, in which three shocks and a contact discontinuity meet at a triple point, is impossible for weak shocks. This apparent disagreement between theory and experiment was pointed out by von Neumann in 1943 and is referred to as the von Neumann, or triple point, paradox [8, 13].

In [13] numerical solutions were obtained of a problem for the unsteady transonic small disturbance equations that describes the reflection of weak shocks off thin wedges. The solutions were obtained in a parameter range where regular reflection is impossible, and contain a sequence of triple points in a tiny region behind the leading triple point, with a centered expansion fan originating at each triple point. It was shown that the triple points with expansion fans observed numerically are in fact consistent with theory, and that the presence of the expansion fans at the triple points resolves the paradox. A solution containing a supersonic patch and an expansion fan was first proposed by Guderley [5, 6]. Although Guderley did not offer evidence that

this is what really occurs nor suggest that there is actually a sequence of expansion fans and triple points to resolve the triple point paradox, the term *Guderley Mach reflection* was chosen in [14] to name this new reflection pattern.

The nonlinear wave system is a simplification of the isentropic Euler equations obtained by dropping the momentum transport terms from the momentum equations [4]. Compared to the unsteady transonic small disturbance equations, the nonlinear wave system is closer in structure to the Euler equations: it is linearly well-posed in space and time, it has a characteristic structure similar to the Euler equations, and change of type takes the equations from a hyperbolic to a mixed-type system. These features make the nonlinear wave system a useful prototype for studying two-dimensional Riemann problems for the full Euler equations.

A problem for the nonlinear wave system that is the analogue of the reflection of weak shocks off thin wedges was studied in [3]. In a parameter range where regular reflection is not possible, the authors showed existence of the subsonic solution behind the Mach shock and reflected wave by solving a free boundary problem for the Mach shock. They did not find the actual reflected shock, but instead based their solution on modeling it as a continuous function with a singularity in the derivative at the sonic boundary. They showed that the composite solution they obtained is not a weak solution near the sonic line. The actual solution, therefore, is different from the construction they present, and they suggest two alternatives. Since triple point solutions do not exist for the nonlinear wave system, one possibility is that the reflected shock is a weak shock that has zero strength at the reflection point. Another possibility is Guderley Mach reflection, as obtained in [13].

Several numerical solutions of the weak shock reflection problem for the nonlinear wave system have been computed. In separate work, R. Sanders, A. Kurganov, and M. Lukacova-Medvidova (all unpublished; see [9]) computed numerical solutions of the problem studied in [3] over a wide range of parameter space where regular reflection is impossible. None of these solutions, however, are sufficiently well resolved to determine the nature of the solution near the apparent triple point. For example, it cannot be determined from any of these solutions whether the reflected shock has zero strength at the triple point, or if some other reflection pattern, such as Guderley Mach reflection, occurs. In fact, in the best resolved of these solutions, three shocks do appear to meet at a triple point—the triple point paradox.

In this paper we present high resolution numerical solutions of the shock reflection problem for the nonlinear wave system. Our most highly resolved solution shows that Guderley Mach reflection occurs at a set of parameter values where regular reflection is impossible: there is a sequence of supersonic patches behind the leading triple point, formed by a sequence of expansion fans and shocks that reflect between the sonic line and the Mach shock. This numerical solution is remarkably similar to those obtained for the unsteady transonic small disturbance equations in [13], and as in [13] the numerical results suggest that the sequence of triple points in an inviscid weak shock Mach reflection may be infinite.

Recent experimental evidence appears to confirm that the resolution of the triple point paradox obtained in [13] and again in the present paper is correct. Skews and Ashworth in [12] obtained schlieren photographs of shock reflection experiments which show a sequence of shocks and expansion waves behind the triple point in a weak shock Mach reflection. The supersonic region is extremely small, as discussed in [13], which is why it had never been observed before. Skews and Ashworth overcame this difficulty by using a specially designed shock tube and flow visualization enhancement techniques.

The numerical solutions of Sanders, Kurganov, and Lukacova-Medvidova were obtained by solving an initial-value problem for the unsteady nonlinear wave system. The problem of inviscid shock reflection off a wedge is self-similar, and there are advantages to solving the problem in self-similar, rather than unsteady, variables. In the unsteady formulation any waves which are present initially move through the numerical domain, making local grid refinement strategies difficult. By contrast, a solution of the self-similar equations is stationary, and local grid refinement near the triple point is much easier to implement. Moreover, in self-similar variables a global grid continuation procedure can be used in which a partially converged solution on a coarse grid is interpolated onto a fine grid, and then driven to convergence on the fine grid. In this paper we present numerical solutions of the shock reflection problem for the nonlinear wave system computed in self-similar coordinates. Procedures for solving the unsteady transonic small disturbance equations in self-similar variables were developed in [13], and are extended here to apply to the nonlinear wave system.

This paper is organized as follows. In section 2 we describe the shock reflection problem for the nonlinear wave system. In section 3 we discuss our approach to solving this problem numerically. The numerical results obtained are presented in section 4. In section 5 we discuss questions raised by our results. Finally, we summarize our findings in section 6.

2. The shock reflection problem for the nonlinear wave system. We consider a problem for the nonlinear wave system that is analogous to the reflection of weak shocks off thin wedges [3]. The shock reflection problem consists of the nonlinear wave system

$$(2.1) \qquad \begin{aligned} \rho_t + (\rho u)_x + (\rho v)_y &= 0, \\ (\rho u)_t + p(\rho)_x &= 0, \\ (\rho v)_t + p(\rho)_y &= 0 \end{aligned}$$

in the half space $x > 0$ with piecewise constant Riemann data consisting of two states separated by a discontinuity located at $x = \kappa y$. Here, $\rho(x, y, t)$ is the density, $u(x, y, t)$ and $v(x, y, t)$ are the x and y components of velocity, respectively, and $p(\rho)$ is the pressure. For convenience, we assume a polytropic gas law

$$p(\rho) = C\rho^\gamma,$$

where C is a constant and γ is the ratio of specific heats. Letting $U = (\rho, m, n)$ denote the vector of conserved variables, where $m = \rho u$ and $n = \rho v$, the Riemann data are

$$(2.2) \qquad U(x, y, 0) = \begin{cases} U_1 \equiv (\rho_1, 0, 0) & \text{if } x < \kappa y, \\ U_0 \equiv (\rho_0, 0, n_0) & \text{if } x > \kappa y. \end{cases}$$

We choose $\rho_0 > \rho_1$ to obtain an upward moving shock in the far field, and determine n_0 so that the one-dimensional wave between U_0 and U_1 at angle κ consists of a shock and a contact discontinuity with a constant middle state between them. The following expression for n_0 was obtained in [3]:

$$(2.3) \qquad n_0 = \frac{1}{\kappa}\sqrt{(1 + \kappa^2)(p(\rho_0) - p(\rho_1))(\rho_0 - \rho_1)}.$$

Strictly speaking, data for reflection from a wedge of angle θ radians would explicitly include the wedge as a discontinuous change of slope, of angle θ, in the boundary

at the point $(0,0)$. In replacing a domain that imitates the physics by a half-plane $(x > 0)$, we are assuming that the reflection pattern near the apparent triple point is a local phenomenon. The physical wedge angle θ in this model is related to κ in (2.2), (2.3) by

$$(2.4) \qquad \theta = \tan^{-1}(1/\kappa).$$

This problem depends on two parameters: the inverse slope κ of the incident shock, and the incident shock strength ρ_0/ρ_1 (see Appendix A). For values of κ greater than a critical value κ_R which depends on ρ_0 and ρ_1, a regularly reflected solution of (2.1)–(2.3) is impossible. In addition, triple point solutions of (2.1), in which three plane shocks separated by constant states meet at a point, do not exist (see Appendix B for a proof of this). We note that a self-similar solution in which three shocks and a linear wave meet at a point can be constructed. However, this is not consistent with the initial data, since (2.1) implies $(m_y - n_x)_t = 0$, even for weak solutions, and slip lines are characterized by nonzero values of $m_y - n_x$. Therefore, Mach reflection cannot occur when regular reflection becomes impossible, and the shock reflection problem for the nonlinear wave system embodies the triple point paradox in an essential form.

The problem (2.1)–(2.3) is self-similar, so the solution depends only on the similarity variables

$$\xi = \frac{x}{t}, \qquad \eta = \frac{y}{t}.$$

We write (2.1) in the form

$$(2.5) \qquad U_t + F_x + G_y = 0,$$

where

$$U = (\rho, m, n), \qquad F = (m, p, 0), \quad \text{and} \quad G = (n, 0, p).$$

Writing (2.5) in terms of ξ, η, and a pseudo-time variable $\tau = \log t$, we obtain

$$(2.6) \qquad U_\tau - \xi U_\xi - \eta U_\eta + F_\xi + G_\eta = 0.$$

As $\tau \to +\infty$, solutions of (2.6) converge to a pseudosteady, self-similar solution that satisfies

$$(2.7) \qquad -\xi U_\xi - \eta U_\eta + F_\xi + G_\eta = 0.$$

Equation (2.7) is hyperbolic when $c^2(\rho) < \xi^2 + \eta^2$, corresponding to supersonic flow in a self-similar coordinate frame, and of mixed type when $c^2(\rho) > \xi^2 + \eta^2$, corresponding to subsonic flow. Here, $c(\rho) = \sqrt{p_\rho}$ denotes the local sound speed. The equation changes type across the sonic line given by

$$(2.8) \qquad \xi^2 + \eta^2 = c^2(\rho).$$

3. The numerical method. In order to solve (2.6) numerically, we write it in conservative form as

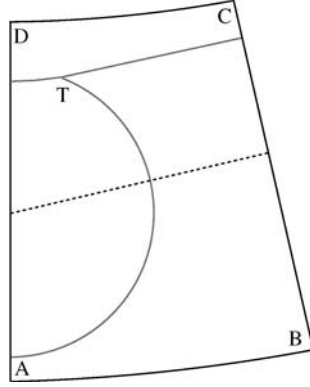$$(3.1) \qquad U_\tau + (F - \xi U)_\xi + (G - \eta U)_\eta + 2U = 0.$$

FIG. 1. *A schematic diagram of the computational domain. AD is the wall and ABCD is the far field numerical boundary. The incident shock enters the computational domain normal to BC. The incident (right of T), reflected (below T), and Mach (left of T) shocks meet at the triple point T.*

In self-similar variables, the nonlinear wave system has the form of the unsteady equations (2.5) with modified flux functions and a lower-order source term.

The essential feature of the numerical method is the capability to locally refine the grid in the area of the apparent triple point. We designed several nonuniform, logically rectangular, finite volume grids so that a given incident shock is aligned with the grid in the far field; see Figure 1. Specifically, each problem with a given incident shock angle has an associated fitted finite volume C-grid. Grid continuation is employed whereby partially converged numerical solutions are quadratically interpolated onto a refined grid. Inside a given box surrounding the triple point, uniform grid spacing is used. Outside of this box, the grid is exponentially stretched in both grid directions.

The basic finite volume scheme is quite standard. Each grid cell, Ω, is a quadrilateral, and using $\vec{\nu} = (\nu_\xi, \nu_\eta)$ to denote the normal vector to a typical side of Ω, numerical fluxes are designed to be consistent with

$$\widetilde{F}(U) = (F(U) - \xi U)\,\nu_\xi + (G(U) - \eta U)\,\nu_\eta = \begin{pmatrix} \nu_\xi m + \nu_\eta n - \bar{\xi}\,\rho \\ \nu_\xi p - \bar{\xi}\,m \\ \nu_\eta p - \bar{\xi}\,n \end{pmatrix},$$

where $\bar{\xi} = (\vec{\xi} \cdot \vec{\nu})$ and $\vec{\xi} = (\xi, \eta)$. Since $\vec{\xi}$ varies, our numerical flux formulae evaluate $\vec{\xi}$ frozen at the midpoint of each cell side. We use two distinctly different numerical fluxes in our results presented below: a first-order Lax–Friedrichs numerical flux and a high-order variant of the Roe numerical flux. The Lax–Friedrichs flux is

$$H_{LF} = \frac{1}{2}\left(\widetilde{F}(U_l) + \widetilde{F}(U_r) - \Lambda\,(U_r - U_l)\right),$$

where $\Lambda > 0$ is a scalar constant chosen to be larger than the fastest wave speed found on the computational domain. While the Lax–Friedrichs method yields only first-order accurate approximations, we regard it to be extremely robust. Our high-order Roe scheme is obtained from piecewise linear reconstruction with characteristic variable limiting, together with the Roe flux

$$H_{Roe} = \frac{1}{2}\left(\widetilde{F}(U_l) + \widetilde{F}(U_r) - R\Lambda L\,(U_r - U_l)\right),$$

where $\Lambda = \mathrm{diag}(|-\bar{\xi}-c|,|-\bar{\xi}|,|-\bar{\xi}+c|)$, and R and L are the matrices of right and left eigenvectors to the Jacobian of $\widetilde{F}$ evaluated at the midpoint $U_{Roe} = \frac{1}{2}(U_l + U_r)$. Below, we use the equation of state $p = 1/2\rho^2$. Therefore, using the midpoint for evaluation yields an exact Roe average since in this case $\widetilde{F}$ is quadratic.

Time integration is accomplished by the forward Euler method for the Lax–Friedrichs scheme:

$$\frac{U^{n+1} - U^n}{\Delta\tau} + \frac{1}{|\Omega|}\int_{\partial\Omega} H_{LF}^n\, ds + 2U^n = 0.$$

For reasons of linear stability, we use the explicit trapezoidal rule to integrate the high-order Roe scheme, as follows:

$$\frac{U^{n+1/2} - U^n}{\Delta\tau} + \frac{1}{|\Omega|}\int_{\partial\Omega} H_{Roe}^n\, ds + 2U^n = 0,$$

$$\frac{2U^{n+1} - U^{n+1/2} - U^n}{\Delta\tau} + \frac{1}{|\Omega|}\int_{\partial\Omega} H_{Roe}^{n+1/2}\, ds + 2U^{n+1/2} = 0.$$

3.1. The grid, initialization, and boundary conditions. We computed solutions of the half-space problem (2.1)–(2.3) in the finite computational domain shown schematically in Figure 1. We use a nonuniform grid that has a locally refined area of uniform grid very close to the triple point, and is stretched exponentially away from the triple point toward the outer numerical boundaries and the wall. (Exponential stretching of 1% means $\Delta x_{i+1} = 1.01\,\Delta x_i$.) In the solutions shown below, the nonuniform grids are stretched by amounts between 0.5% and 1%. The total number of grid points in our largest grid is approximately 11×10^6, of which approximately 2.5×10^6 cover a very small region surrounding the triple point. (See Figure 3(c) below where this small region is depicted.)

We impose reflecting boundary conditions, equivalent to the physical no-flow condition, on the wall AD. A standard first-order ghost cell implementation, with fictitious cells located to the left of the boundary AD, is given by

$$(3.2) \qquad\qquad \begin{aligned} \rho_{-1} &= \rho_0, \\ m_{-1} &= -m_0, \\ n_{-1} &= n_0, \end{aligned}$$

where the subscripts -1 and 0 indicate values at ghost cells and at the first real cell adjacent to the boundary, respectively. In our higher-order computations we used a second-order formulation of this boundary condition. In addition, we require numerical boundary conditions on the outer computational boundaries.

In [3] expressions were given for the one-dimensional wave between U_0 and U_1 in the far field. The constant middle state $U_m = (\rho_0, m_m, n_m)$ between the contact discontinuity (the dotted line in Figure 1), located at $\xi = \kappa\eta$, and the incident shock, located at $\xi = \kappa\eta + \chi$, is given by

$$(3.3) \qquad\qquad \begin{aligned} m_m &= -\sqrt{\frac{(p(\rho_0) - p(\rho_1))(\rho_0 - \rho_1)}{1 + \kappa^2}}, \\ n_m &= -\kappa m_m, \\ \text{with}\quad \chi &= -\sqrt{1 + \kappa^2}\sqrt{\frac{p(\rho_0) - p(\rho_1)}{\rho_0 - \rho_1}}. \end{aligned}$$

On the outer numerical boundary $ABCD$, we impose Dirichlet data corresponding to the incident shock/contact discontinuity solution in (2.2), (2.3), (3.3). We find that

$$(3.4) \qquad U(\xi, \eta) = \begin{cases} U_1, & \xi < \kappa\eta + \chi, \\ U_m, & \kappa\eta + \chi < \xi < \kappa\eta, \\ U_0, & \xi > \kappa\eta. \end{cases}$$

We impose (3.4) as a boundary condition for (3.1) on $ABCD$.

4. Numerical results. We computed numerical solutions of (2.1)–(2.3) for κ equal to 1, 2, 4, and 8. In our computations we used ρ_0/ρ_1 equal to 64, 8, and 2. In the following figures we present solutions with $\rho_1 = 1$ and ρ_0/ρ_1 equal to 64. The solutions for other values of ρ_0/ρ_1 are similar to the ones presented here. For all computations, the polytropic gas law $p = \frac{1}{2}\rho^2$ was used. Figure 2 shows ρ-contour plots of the global solutions as a function of $(x/t, y/t)$. From (2.4), increasing κ corresponds to decreasing the wedge angle that is modeled by our problem. Hence, the sequence of plots in Figure 2(a)–(d) is a numerical representation of a series of shock reflection experiments in which the wedge angle is decreased, while holding the shock strength ρ_0/ρ_1 constant.

The numerical solutions appear to show a simple Mach reflection, with three shocks meeting at a triple point. The Mach shock becomes longer and weaker as κ increases, and the strength of the reflected shock also decreases when κ increases. For a fixed value of κ, the strength of the Mach shock increases as it moves away from the triple point, reaching a maximum at the wall $x = 0$.

For the value $\kappa = 1$, we used local grid refinement to obtain a highly resolved solution in the neighborhood of the triple point. In Figure 3(a)–(c), we show ρ-, m-, and n-contours and the numerically computed location of the sonic line, equation (2.8), near the triple point for $\kappa = 1$. The solution contains a small region of supersonic flow behind the triple point. The width $\Delta(x/t)$ of the patch is approximately 0.03, and the height $\Delta(y/t)$ is approximately 0.01. Here, the width $\Delta(x/t)$ is a numerical estimate of the difference between the maximum value of x/t on the sonic line and the minimum value of x/t at the rear sonic point on the Mach shock. The height $\Delta(y/t)$ is an estimate of the difference between the value of y/t at the triple point and the minimum value of y/t at the rear sonic point on the Mach shock. The width of the supersonic region is approximately 5% of the length of the Mach shock. The expansion fan centered at the leading triple point can be clearly seen. Behind the leading triple point, there is a sequence of shocks and expansion fans. The thickening of the incident shock as it moves away from the triple point in Figure 3(a)–(c) is caused by the use of a stretched grid.

The area covered by the most refined uniform grid is indicated by the box contained in Figure 3(c), and the figure caption gives the number of grid points in the most refined area of the grid. The box appears to be skewed because of the use of a C-grid. To illustrate the size and location of the refined uniform grid, in Figure 3(d) we plot ρ-contour lines over the entire numerical domain, for $\kappa = 1$. The refined grid area is too small to be visible in the main plot shown in Figure 3(d). The inset figure shows an enlargement of the solution contained within the small rectangular box centered about the reflection point, as indicated. The solution shown in the inset figure also contains a small box centered at the reflection point, indicating the approximate size and location of the region shown in Figure 3(a)–(c).

We found that, as in [13], a certain minimum grid resolution was required to resolve the supersonic region behind the triple point. As we refined the grid beyond
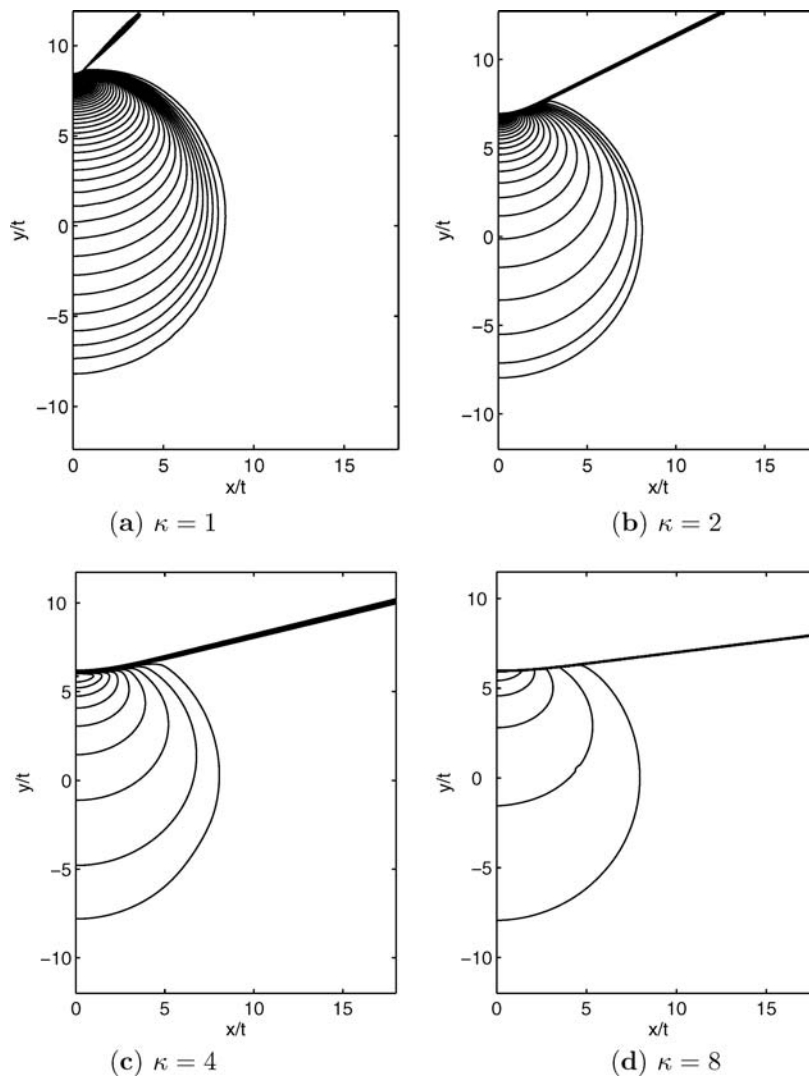
FIG. 2. *Contour plots of ρ for increasing values of κ. The ρ-contour spacing is* 1.0. *The shock strength $\rho_0/\rho_1 = 64$; $\rho_1 = 1$.*

this minimum level, details of the flow field near the triple point became clearer. Figure 4 shows ρ-contours and the sonic line near the triple point for a sequence of solutions for $\kappa = 1$, using a Lax–Friedrichs numerical flux. The sequence was computed using successively refined grids, with each grid refined by a factor of two in x/t and y/t in relation to the previous grid. The resolution of the locally refined areas is indicated on the plots. In Figure 4(a)–(b), the sonic line appears smooth. At the next level of refinement, shown in Figure 4(c), there is a steepening of the contours at the rear of the patch, and an indication of a shock forming there. Further shocks appear in our highest resolution solution in Figure 3. At resolutions lower than shown in the figure, the supersonic region disappears entirely.

There is a small discrepancy between the location of the triple point in these figures and the theoretical location of the incident shock, given in (3.3). The reason for
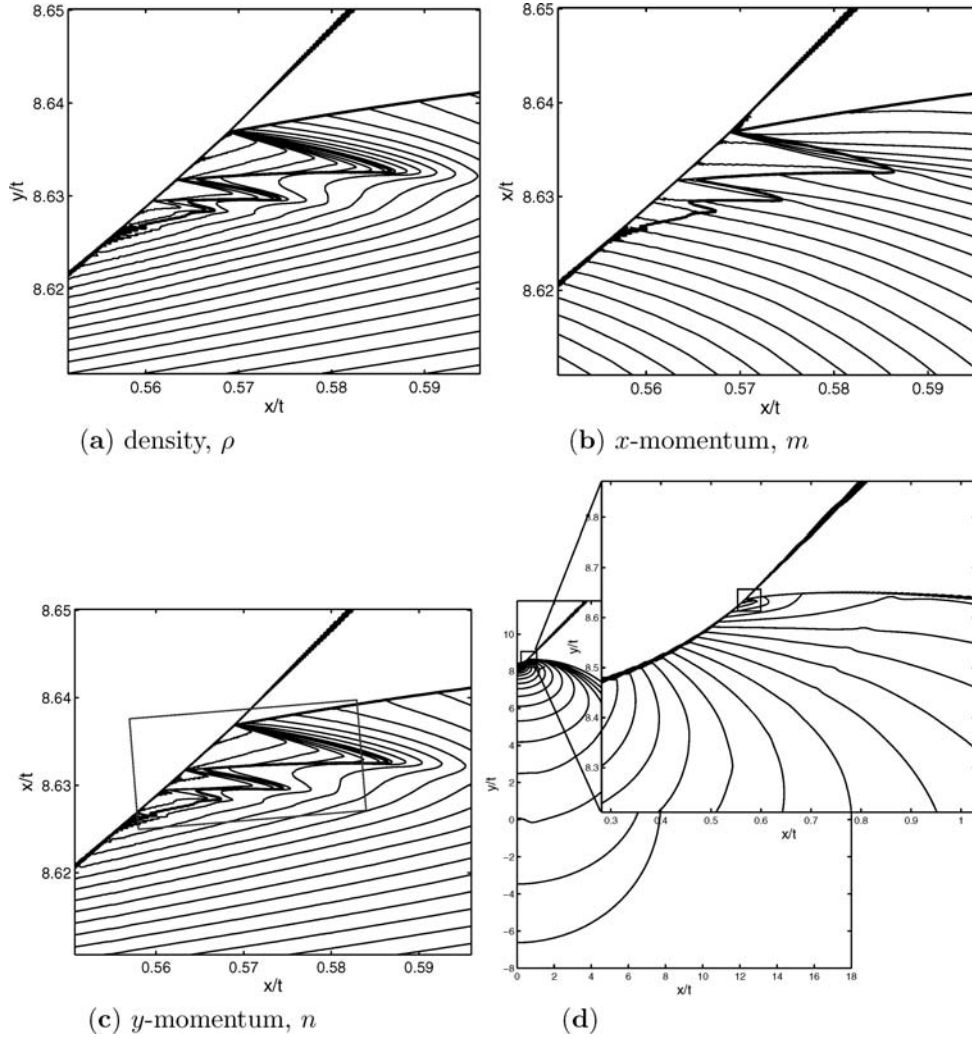
(a) density, ρ

(b) x-momentum, m

(c) y-momentum, n

(d)

FIG. 3. *The contour plots in* (a)–(c) *show the true nature of the solution near the triple point for* $\kappa = 1$. *The* ρ-*contour spacing is 0.5 in* (a), *the* m-*contour spacing is 1.5 in* (b), *and the* n-*contour spacing is 5.25 in* (c). *The heavy line is the sonic line. The box in* (c) *indicates the area of the refined uniform grid, which has* 2048×1320 *grid points. A second-order Roe numerical flux was used. The plot in* (d) *is an illustration of the approximate size and location of the region shown in the plots in* (a)–(c), *which is contained in the small rectangular box shown in the inset figure; the plot shows contour lines of* ρ.

the discrepancy is that the numerical boundary conditions did not give an incident shock that was of exactly constant strength and exactly straight in the $(x/t, y/t)$ coordinates. However, the deviation of the numerical solution for the incident shock from the exact uniform solution was small. For example, in our numerical solution shown in Figure 3, the numerically computed value of the y/t coordinate of the triple point differs by 0.1% from the theoretical value obtained from (3.3) using the numerically computed value of x/t, and the nonuniformity in ρ in the state behind the incident shock near the triple point is about 0.6%. We tried a number of different implementations of the numerical boundary conditions and computational mesh, but none of
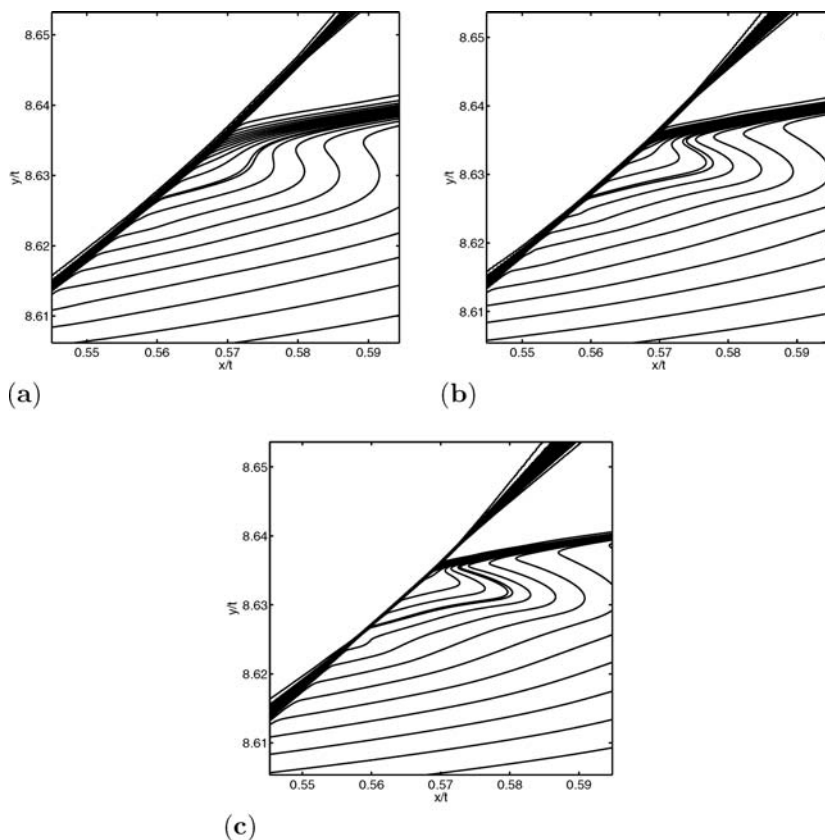
FIG. 4. *A sequence of contour plots illustrating the effect of increasing grid resolution on the numerical solution. The solutions plotted here are for $\kappa = 1$. The figures show ρ-contours in the refined grid area near the triple point, with a ρ-contour spacing of 1.0. Each grid is refined by a factor of two in relation to the previous grid. The region shown includes the refined uniform grid area. The heavy line is the sonic line. In* (a), *the refined uniform grid contains 760×760 grid points. A supersonic region is visible as a bump in the sonic line, but it is poorly resolved. In* (b), *the refined uniform grid area contains 1280×1024 grid points. The supersonic region appears to be smooth. In* (c), *the refined uniform grid area contains 2048×1320 grid points. There is an indication of an expansion fan behind the leading triple point.*

them gave an incident shock that was of exactly constant strength. Nevertheless, the presence of a supersonic patch did not depend on the particular implementation.

In the computation for $\kappa = 1$, we partially converged a solution on a coarse grid, resampled the data onto a refined grid, and repeated the process until the necessary resolution was obtained. Three consecutive intermediate solutions in this computation are shown in Figure 4. Computations on less refined grids were made using a Lax–Friedrichs numerical flux, and after partial convergence on the most refined grid we switched to the more expensive Roe method. Figure 5 shows ρ-contours for a solution made using a first-order Roe scheme. Further computation using a second-order Roe scheme yielded the final solution shown in Figure 3. The solution on the final grid was evolved until no further change was observed in the details of the solution near the triple point. The solutions shown in Figures 4(c), 5, and 3 were obtained on the same grid using different methods. All three of the solutions contain a small supersonic region behind the triple point. The solutions shown in Figures 5 and 3,
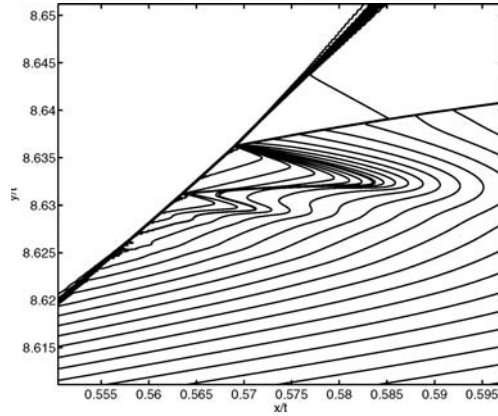
FIG. 5. *A contour plot of ρ near the triple point computed using a first-order Roe method. The number of points in the refined uniform grid is the same as in Figure 4, which shows a Lax–Friedrichs solution, and in Figure 3(a)–(c), which shows a second-order Roe method solution. The ρ-contours are plotted at the same levels of ρ as in Figure 3(a).*
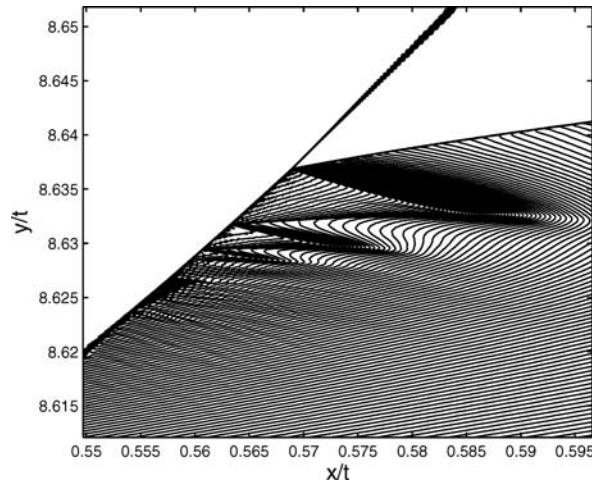

FIG. 6. *A detailed plot of contour lines for ρ illustrating Guderley Mach reflection. The ρ-contour spacing is 0.1. Three reflected shock/expansion wave pairs are clearly visible, with indications of a fourth. The region shown contains the refined uniform grid, which has 2048×1320 grid points.*

which are more highly resolved, contain a sequence of supersonic patches and triple points, which is better defined in Figure 3.

In Figure 6 we plot closely spaced ρ-contours to give a detailed picture of the sequence of shocks and expansion waves in a Guderley Mach reflection for $\kappa = 1$. Each shock-expansion pair in the sequence is smaller and weaker than the one preceding it. Three reflected shocks appear to be visible in the plot. From the numerical data, their approximate strengths, beginning with the leading reflected shock, are given in Table 1. The jump $[\rho]$ in ρ across a reflected shock is measured near the point where the flow behind the shock is sonic. This point is very close to the corresponding triple point on the Mach shock, as shown in Figure 3.

Approximate values of the reflected shock strengths for the three reflected shocks visible in Figure 6, beginning with the leading reflected shock, from the numerical data. For each shock, ρ_1 and ρ_0 denote the approximate values of ρ ahead of and behind the shock, respectively.

Shock	ρ_1	ρ_0	$[\rho]$
1	64	76	12
2	72	75	3
3	74	75	1

5. Discussion. These numerical results are remarkably similar to the computed solutions of the shock reflection problem for the unsteady transonic small disturbance equations in [13]. In both cases, a weak shock reflection in a parameter range where regular reflection is impossible results in a sequence, possibly infinite, of triple points and supersonic patches embedded in the subsonic flow behind the Mach and reflected shocks. The unsteady transonic small disturbance equations can be derived from the full Euler equations by a systematic asymptotic expansion, and are considered to give an adequate description of the physical flow near the shock interaction point for weak shocks and small wedge angles. The nonlinear wave system, however, is not a systematic reduction of the Euler equations, and it does not appear to have any immediate physical relevance. It is therefore noteworthy that the shock reflection problem for the nonlinear wave system has a solution that resembles the solutions in [13], and is consistent with the experimental results in [12].

The nonlinear wave system has a characteristic structure similar to the two-dimensional Euler equations: nonlinear acoustic waves coupled (weakly) with linearly degenerate waves. The nonlinear wave system also respects the spatial (Euclidean) symmetries of gas dynamics, but not the space-time (Galilean) symmetry. In fact (see [10]), they are essentially the simplest system one can construct with these symmetries. The existence of a Guderley Mach reflection solution for a system that is only loosely related to gas dynamics suggests that the behavior may be typical of equations with this characteristic structure, and is not restricted to equations that describe gas dynamic phenomena. We conjecture that a sequence of supersonic patches and triple points is a generic feature of two-dimensional Riemann problems for some class of hyperbolic systems of conservation laws. Possibly this class is characterized by "acoustic waves," as defined in [2]. It is possible that numerical solutions of the weak shock reflection problem for the full Euler equations will contain a sequence of supersonic patches as well.

An important feature of the numerical solution is the small size of the supersonic region. In our solution for $\kappa = 1$, the width of the supersonic patch is approximately 5% of the length of the Mach shock. This is somewhat larger than the supersonic regions in the solutions in [13], which were obtained over a range of parameter values and varied in height from approximately 0.05% to 3% of the length of the Mach shock. Based on the dependence of patch size on wedge angle observed in [13], we expect solutions for larger values of κ to contain even larger supersonic regions. However, the strength of the reflected shock near the triple point decreases as κ increases, making it very difficult to resolve numerically the details of the solution near the triple point. We have displayed a solution with $\kappa = 1$ because it offers a good compromise between the size of the supersonic region and the strength of the sequence of reflected shocks and expansions.

One of the scenarios proposed in [3] for resolving the triple point paradox in the nonlinear wave system is that the reflected shock have zero strength at the shock

interaction point. In that case, there would be no triple point, and presumably no supersonic patch. We have obtained solutions, using different numerical schemes, which contain a supersonic region behind the triple point in a weak shock reflection. In these solutions, the reflected shocks have finite strength at the point where they collide with the Mach shock. Although we have not obtained numerical evidence of the zero strength reflected shock solution, we note that in the problem studied in [3], it is assumed that κ is large enough that the incident shock intersects the sonic circle, equation (2.8), corresponding to the state U_0 behind the shock. For shock reflection data with $\kappa = 1$, the incident shock does not intersect the sonic circle, so the partial solution presented in [3] is not available here. We also note, however, that in [13], several solutions were obtained in a parameter range for which the incident shock does intersect the sonic line for the state behind the incident shock. All of these solutions contained a reflected shock of nonzero strength at the triple point, and a supersonic region. For the nonlinear wave system, since we have obtained a solution containing a supersonic region at only one set of parameter values, we do not know if Guderley Mach reflection occurs over the entire set of parameter values for which regular reflection is impossible, or if solutions at large enough values of κ contain a reflected shock with zero strength at the triple point.

6. Conclusion. We have presented numerical evidence of a structure of reflected shocks and expansion waves, and a sequence of triple points and supersonic patches, in a small region behind the leading triple point in a shock reflection problem for the nonlinear wave system. This result is consistent with previous numerical solutions of a shock reflection problem for the unsteady transonic small disturbance equations, and with recent experimental results for weak shocks reflecting off thin wedges.

Appendix A. Symmetry. Equation (2.1) admits the usual Euclidean symmetries of gas dynamics (translation invariance and equivariance under rotation and reflection in the plane), but not the Galilean symmetry. For a polytropic gas law $p(\rho) = C\rho^\gamma$, where γ is the ratio of specific heats and C is a constant, it is also invariant under the scaling

$$(x, y) \mapsto \rho_1^{\frac{\gamma-1}{2}}(x, y), \qquad \rho \mapsto \rho_1\rho, \qquad (m, n) \mapsto \rho_1^{\frac{\gamma+1}{2}}(m, n).$$

Based on this, we see that solutions of the nonlinear wave system depend on the density only through a characteristic density ratio ρ_0/ρ_1, or equivalently, through the velocity ratio or the Mach number $M = c(\rho_0)/c(\rho_1) = (\rho_0/\rho_1)^{(\gamma-1)/2}$.

Appendix B. Nonexistence of triple points. To examine triple points in the nonlinear wave system we note, first, that this system does not have the Galilean invariance of the gas dynamics equations, so we cannot assume that the flow is stationary at a triple point. However, because of rotational symmetry we can assume that one of the shocks is horizontal, and we do so to simplify the calculation. We can also choose one set of momentum components to be zero.

We label the horizontal shock S_a, and proceeding counterclockwise, the other two are S_b and S_c (Figure 7). The state between S_a and S_b is $U_1 = (\rho_1, 0, 0)$; the other two states, also proceeding counterclockwise, are U_2 and $U_0 = (\rho_0, 0, n_0)$. The value of ρ_0 can be any number greater than ρ_1. Note that the component $m_0 = 0$ because S_a is horizontal. The equation of S_a is $\{\eta = \omega_a\}$, where $\omega_a = \sqrt{(p_0 - p_1)/(\rho_0 - \rho_1)}$, and $n_0 = \omega_a[\rho] = \sqrt{(p_0 - p_1)(\rho_0 - \rho_1)}$, using (2.3). (Note that $\kappa_a = \infty$ here and that U_0 corresponds to U_m in (3.3).)
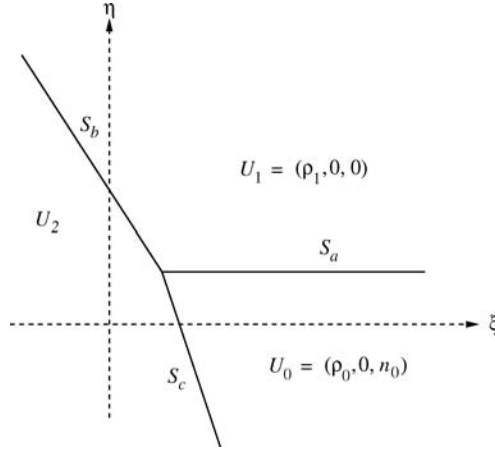
FIG. 7. *Triple point configuration.*

We introduce the notation $P_{ab} = \sqrt{(p_a - p_b)(\rho_a - \rho_b)}$. We have the following proposition.

PROPOSITION B.1. *For any convex equation of state $p(\rho)$, there is no nontrivial set of solutions to the Rankine–Hugoniot equations for constant states $\{U_0, U_1, U_2\}$ separated by shocks S_a, S_b, S_c, irrespective of whether the three shocks intersect in a point or not.*

Proof. The Rankine–Hugoniot equations at S_b and S_c imply (see [4, Appendix A])

$$m_2 - m_1 = \frac{P_{21}}{\sqrt{1 + \kappa_b^2}}, \qquad m_2 - m_0 = \frac{P_{20}}{\sqrt{1 + \kappa_c^2}},$$

$$n_2 - n_1 = -\frac{P_{21}}{\sqrt{1 + \kappa_b^2}}\kappa_b, \qquad n_2 - n_0 = -\frac{P_{20}}{\sqrt{1 + \kappa_c^2}}\kappa_c.$$

Using the values $m_1 = m_0 = n_1 = 0, n_0 = P_{01}$, we get two equations:

(B.1) $\qquad m_2 = \frac{P_{21}}{\sqrt{1 + \kappa_b^2}} = \frac{P_{20}}{\sqrt{1 + \kappa_c^2}}, \qquad n_2 = -\frac{P_{21}}{\sqrt{1 + \kappa_b^2}}\kappa_b = P_{01} - \frac{P_{20}}{\sqrt{1 + \kappa_c^2}}\kappa_c.$

In principle, we can solve this pair of equations to obtain κ_b and κ_c as functions of the data ρ_0 and ρ_1. We get a 1-parameter family of solutions parameterized by ρ_2. However, the solutions obtained are not real numbers. For, if we substitute the first equation in (B.1) into the second, we get

$$-\kappa_b \frac{P_{20}}{\sqrt{1 + \kappa_c^2}} = P_{01} - \kappa_c \frac{P_{20}}{\sqrt{1 + \kappa_c^2}},$$

or

(B.2) $$\kappa_b = \kappa_c - \sqrt{1 + \kappa_c^2}\frac{P_{01}}{P_{20}}.$$

Now square the first relation in (B.1), write it as

$$1 + \kappa_b^2 = (1 + \kappa_c^2)\frac{P_{21}^2}{P_{20}^2},$$

and substitute (B.2), to obtain

$$1 + \left(\kappa_c - \sqrt{1 + \kappa_c^2} \frac{P_{01}}{P_{20}} \right)^2 = (1 + \kappa_c^2) \frac{P_{21}^2}{P_{20}^2},$$

or

$$(P_{20}^2 + P_{01}^2 - P_{21}^2) \sqrt{1 + \kappa_c^2} = 2 \kappa_c P_{01} P_{20}.$$

Square this and solve for κ_c^2:

$$\kappa_c^2 = \frac{(P_{20}^2 + P_{01}^2 - P_{21}^2)^2}{4 P_{01}^2 P_{20}^2 - (P_{20}^2 + P_{01}^2 - P_{21}^2)^2}.$$

Now, after a calculation,

$$P_{20}^2 + P_{01}^2 - P_{21}^2 = (\rho_2 - \rho_0)(p_1 - p_0) + (\rho_1 - \rho_0)(p_2 - p_0).$$

So

$$4 P_{01}^2 P_{20}^2 - (P_{20}^2 + P_{01}^2 - P_{21}^2)^2 = -[(\rho_2 - \rho_0)(p_1 - p_0) - (\rho_1 - \rho_0)(p_2 - p_0)]^2 \le 0.$$

In fact, this quantity is less than zero unless

$$\frac{p_2 - p_0}{\rho_2 - \rho_0} = \frac{p_1 - p_0}{\rho_1 - \rho_0}.$$

For a convex function p, this implies $\rho_2 = \rho_1$, a degenerate case with only two distinct states.

Thus, no solutions exist. Note that the proof did not require the three shocks to intersect in a point, and that therefore this is a somewhat stronger result than simply the nonexistence of triple points.   □

In a similar manner it is possible to show that, as in gas dynamics, a self-similar solution consisting of three shocks and a linear wave meeting at a point can be constructed. However, as mentioned in section 2, because of the invariance in time of the quantity $(m_y - n_x)$, the linear characteristic coordinate, a linear wave cannot be present in the solution unless it is present in the data. For the data given in (2.2), therefore, solutions containing a triple point with a linear wave cannot exist. The same triple point paradox occurs in gas dynamics, of course, where solutions containing a triple point with a contact discontinuity cannot occur for sufficiently weak shocks (see [7] for a discussion of this).

REFERENCES

[1] M. BRIO AND J. K. HUNTER, *Mach reflection for the two-dimensional Burgers equation*, Phys. D, 60 (1992), pp. 194–207.

[2] S. ČANIĆ AND B. L. KEYFITZ, *Quasi-one-dimensional Riemann problems and their role in self-similar two-dimensional problems*, Arch. Ration. Mech. Anal., 144 (1998), pp. 233–258.

[3] S. ČANIĆ, B. L. KEYFITZ, AND E. H. KIM, *Free boundary problems for nonlinear wave systems: Mach stems for interacting shocks*, SIAM J. Math. Anal., 37 (2006), pp. 1947–1977.

[4] S. ČANIĆ, B. L. KEYFITZ, AND E. H. KIM, *Mixed hyperbolic-elliptic systems in self-similar flows*, Bol. Soc. Bras. Mat., 32 (2001), pp. 1–23.

[5] K. G. GUDERLEY, *Considerations of the Structure of Mixed Subsonic-Supersonic Flow Patterns*, Air Materiel Command Tech. Report, F-TR-2168-ND, ATI 22780, GS-AAF-Wright Field No. 39, U.S. Wright-Patterson Air Force Base, Dayton, OH, 1947.

[6] K. G. GUDERLEY, *The Theory of Transonic Flow*, Pergamon Press, Oxford, UK, 1962.

[7] L. F. HENDERSON, *Regions and boundaries for diffracting shock wave systems*, Z. Angew. Math. Mech., 67 (1987), pp. 73–86.

[8] J. K. HUNTER AND M. BRIO, *Weak shock reflection*, J. Fluid Mech., 410 (2000), pp. 235–261.

[9] B. L. KEYFITZ, home page, http://www.math.uh.edu/∼blk.

[10] B. L. KEYFITZ AND M. C. LOPES FILHO, *A geometric study of shocks in equations that change type*, J. Dynam. Differential Equations, 6 (1994), pp. 351–393.

[11] J. VON NEUMANN, *Collected Works*, Vol. 6, Pergamon Press, New York, 1963.

[12] B. SKEWS AND J. ASHWORTH, *The physical nature of weak shock wave reflection*, J. Fluid Mech., 542 (2005), pp. 105–114.

[13] A. M. TESDALL AND J. K. HUNTER, *Self-similar solutions for weak shock reflection*, SIAM J. Appl. Math., 63 (2002), pp. 42–61.

[14] J. K. HUNTER AND A. M. TESDALL, *Weak shock reflection*, in A Celebration of Mathematical Modeling, D. Givoli, M. Grote, and G. Papanicolaou, eds., Kluwer Academic, New York, 2004.